Synthesis and characterization of $Ba_3(Pb_{1-x}Bi_x)_2O_7$

R. J. Cava and H. Takagi
AT&T Bell Laboratories, Murray Hill, New Jersey 07974

H. W. Zandbergen
National Centre for High Resolution Electron Microscopy, Technical University, Delft, The Netherlands

B. Hessen, J. J. Krajewski, and W. F. Peck, Jr.
AT&T Bell Laboratories, Murray Hill, New Jersey 07974
(Received 18 June 1992)

The synthesis and initial characterization of a layered perovskite-based lead-bismuth oxide are reported. The phase, $Ba_3(Pb_{1-x}Bi_x)_2O_7$, for $0 \le x \le 0.5$, is the $n=2$ member of the Ruddlesden-Popper series $A_{n+1}B_nO_{3n+1}$. It can be synthesized only under very narrowly defined conditions. Despite the analogy to the well-known three-dimensional perovskite superconductor $BaPb_{0.75}Bi_{0.25}O_3$, layered $Ba_3Pb_2O_7$ does not become superconducting (down to 1.8 K) on doping with Bi.

INTRODUCTION

The $BaPbO_3$-$BaBiO_3$–based perovskite superconductors, with T_c's ranging from 3.5 K ($BaPb_{0.75}Sb_{0.25}O_3$) to 31 K ($Ba_{0.6}K_{0.4}BiO_3$) remain enigmatic materials. The discussion involves whether or not they are conventional electron-phonon-coupled superconductors or are good examples of an electronically driven coupling mechanism.[1–6] Three-dimensionally connected and nonmagnetic, they stand in considerable contrast to high-T_c copper oxides. Superconductivity has not been observed for this family in any but the simple ABO_3 perovskite structure type. Unlike copper-oxide-based perovskites, very few potentially superconducting compounds are even known. The layered compounds Ba_2PbO_4, $Ba_4Pb_3O_{10}$, and $Ba_{1.7}K_{1.3}Bi_2O_7$ have not been made superconducting.[7–10] Here we report the synthesis and initial characterization of the compound and solid solution $Ba_3(Pb_{1-x}Bi_x)_2O_7$, which, like $(Ba,K)_3Bi_2O_7$, has a double layer of (Pb,Bi)-O octahedra. It has not been prepared as a bulk phase previously due to the existence of a narrow temperature region where it can be synthesized. Resistivity measurements show that $Ba_3Pb_2O_7$ is a poorly conducting metal and becomes more resistive on Bi doping. None of the compositions becomes superconducting above 1.8 K.

SYNTHESIS

Optimal starting materials for synthesis were $Ba(NO_3)_2$, $Pb(NO_3)_2$, and Bi_2O_3. Powders were mixed in the stoichiometric metal ratios for $Ba_3(Pb_{1-x}Bi_x)_2O_7$ with $0 \le x \le 0.7$, at intervals $\Delta x = 0.1$. They were then mechanically ground for 30 min. They were heated at 100 °C per h in oversize dense Al_2O_3 crucibles and soaked at 800 °C, all in flowing O_2, for 5 h. Extended heating at 800 °C was detrimental, as it resulted in the formation of the $Ba_4Pb_3O_{10}$-type phase, which is much more stable than the phase of interest. After mechanical grinding for another 30 min, 1-g pills were pressed for the final synthetic step. To find the optimal synthetic temperature, pills were first heated for several days in O_2 at 890–970 °C in $\Delta T = 10$ °C intervals, inserted directly into, and removed directly from, a hot furnace. The pure $Ba_3(Pb_{1-x}Bi_x)_2O_7$ phase was obtained only at 910 and 930 °C, the other temperatures showing this phase plus the $Ba_4Pb_3O_{10}$-type phase. Final best results were obtained for samples which had been inserted into a vertical furnace already at 930 °C, heated for 50–60 h in O_2, and quenched by dropping from the hot zone. Surprisingly, although single-phase materials could be made for $x=0$ and $0.2 \le x \le 0.5$, we could not find conditions which made $x=0.1$ single phase. All single-phase materials were finally heated at 450 °C in O_2 for 14 h.

STRUCTURAL CHARACTERIZATION

The powder x-ray-diffraction pattern for $Ba_3Pb_2O_7$ is presented in Table I. It can be indexed by a body-centered tetragonal unit cell with $a=4.29$ and $c=21.7$ Å, as would be expected for the $n=2$ member of the series $Ba_{n+1}Pb_nO_{3n+1}$. Electron diffraction, however, shows the presence of a weak $\sqrt{2}a_p$ superlattice, and so $a \cong \sqrt{2} \times 4.29$ is the true cell parameter. Table II presents the variation in lattice parameter on Bi doping in the solid solution $Ba_3(Pb_{1-x}Bi_x)_2O_7$, obtained by least-squares fitting to the positions of 20–25 lines in the powder diffraction patterns (Cu $K\alpha$ radiation) between 0° and 80° 2θ. The variation of the crystallographic cell parameters and cell volume with Bi content is shown in Fig. 1, for the perovskite-like subcell. If the parameters for the Bi-doped samples are extrapolated to $Ba_3Pb_2O_7$, that phase does not appear to occur at the expected cell parameters, which could be a symptom of the immiscibility at $x=0.1$. More precise lattice parameter measurements would be necessary to confirm the discontinuity suggested in Fig. 1. As in the solutions $BaPb_{1-x}Bi_xO_3$ and $Ba_4(Pb_{1-x}Bi_x)_3O_{10}$, the unit-cell volume increases on Bi doping.

Thin specimens for electron microscopy were obtained

TABLE I. Powder x-ray-diffraction pattern of $Ba_3Pb_2O_7$ (Cu $K\alpha$). $a = 6.071(3)$ Å, $c = 21.732(7)$ Å.

	Tetragonal		
Index	$2\theta_{obs}$ (deg)	$2\theta_{calc}$ (deg)	I/I_0
002	8.10	8.13	4
004	16.28	16.30	5
111	21.05	21.08	3
115	29.23	29.22	100
204	33.80	33.80	2
117	35.63	35.66	3
0010	41.50	41.52	13
220	42.08	42.06	51
222	42.91	42.92	6
224	45.39	45.40	1
131	47.54	47.51	1
1111	50.90	50.83	5
2010	51.69	51.69	16
135	52.03	52.03	33
137	56.27	56.30	2
2012	59.39	59.37	3
2210	60.60	60.58	15
400	60.96	61.00	6
402	61.63	61.66	3
1115	68.24	68.26	6
0016	69.11	69.09	13
2214	75.51	75.52	3
4010	76.54	76.49	6
1117	77.88	77.90	4

by crushing and mounting the crystal fragments on a Cu grid covered with a carbon-coated holey film. Electron microscopy was performed with a Phillips CM30ST electron microscope operating at 300 kV and equipped with side-entry 25°/25° tilt specimen holder. The high resolution electron microscopy (HREM) images were recorded at a series of defocus values, and, in particular, at a defocus of about -40 nm at which all cations in [110] images are imaged as dark dots. Image calculations were carried out using a MacTempas software program, in which the following parameters were used: Cs is 1.2 mm, defocus spread is 9 nm, objective aperture is 6.5 nm^{-1}, beam convergence 1.2 mrad, and mechanical vibration 0.05 nm. The thickness and defocus were varied. Several experimental HREM images were averaged over a number of unit cells to improve the ability to measure gray values of the various positions and the actual positions of the black dots. Images were digitized with about 50 pixels per nm. These images were noise reduced by first averaging each

TABLE II. Crystallographic characterization of $Ba_3(Pb_{1-x}Bi_x)_2O_7$ (tetragonal symmetry).

x	a_0 (Å)	a_p[a] (Å)	c_0 (Å)	Vol_p[a]
0.0	6.071(3)	4.293(2)	21.732(7)	400.5(4)
0.2	6.086(3)	4.304(2)	21.795(7)	403.7(5)
0.3	6.096(4)	4.311(3)	21.814(11)	405.4(8)
0.4	6.099(4)	4.313(3)	21.827(12)	406.0(8)
0.5	6.106(4)	4.318(3)	21.859(12)	407.6(8)

[a]For a simple perovskite-like $a_0/\sqrt{2}$ subcell.

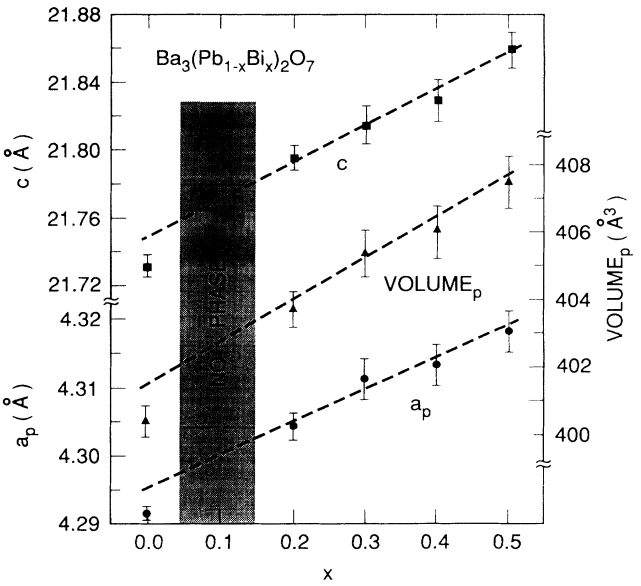

FIG. 1. Variation of the crystallographic cell parameters ($I4/mmm$ perovskite-like subcell) with Bi content in $Ba_3(Pb_{1-x}Bi_x)_2O_7$.

pixel over itself and its eight neighbors and next by averaging the image over a number of unit cells.

Electron diffraction was carried out with a number of crystallites, which were rotated to scan the reciprocal space. Electron-diffraction patterns of the [100], [110], and [001] orientations are shown in Fig. 2. Superreflections indicating a tetragonal $a_p\sqrt{2}$, $a_p\sqrt{2}$, c superstructure can be observed in the [100] diffraction

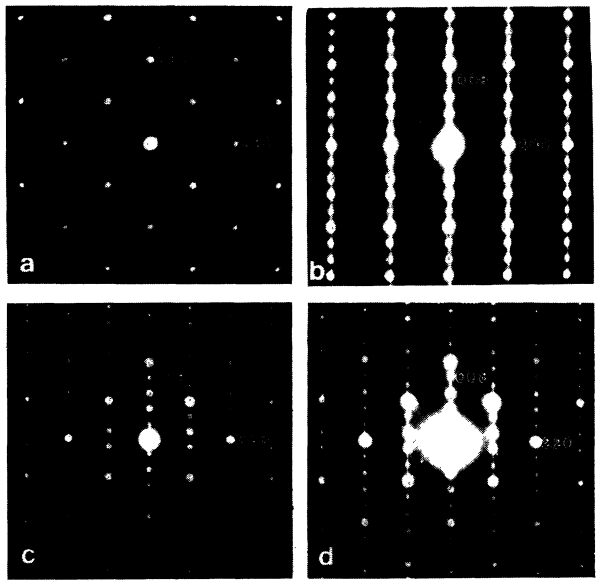

FIG. 2. Electron-diffraction patterns along (a) [001], (b) [100], (c) [110], and (d) [110]. Note the superstructure along the c^* axis in (d), which probably corresponds to a stacking of five units of $Ba_3Pb_2O_7$ and one unit of $Ba_4Pb_3O_{10}$. Streaking corresponding to irregular stacking defects can be seen in (b) and (c).

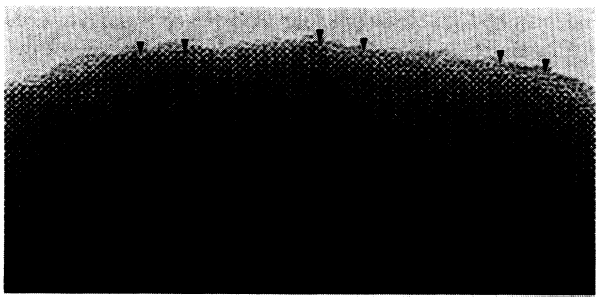

FIG. 3. [110] micrographs showing the presence of a stacking defects corresponding to a composition $Ba_4Pb_3O_{10}$ (arrows) in a matrix of $Ba_3Pb_2O_7$. Note that the defects in the matrix have a regular sequence $[6x(Ba_3Pb_2O_7)1x(Ba_4Pb_3O_{10})1x(Ba_3Pb_2O_7)1x(Ba_4Pb_3O_{10})]_n$.

pattern, leading to a unit cell of $a \cong b \cong 6.0$ and $c \cong 21.6$ Å. The systematic absences of the substructure reflections indicate the basic structure to have an I-centered symmetry. Some streaking along the c^* axis was observed in most of the crystallites, indicating planar defects along the c axis.

HREM showed the planar defects to be predominantly of the composition $Ba_4Pb_3O_{10}$, an example of which can be seen in Fig. 3. Some crystallites of almost single phase $Ba_4Pb_3O_{10}$ were observed. Figure 4 shows a high-resolution image of the bulk material. A good agreement is obtained with calculated images using the structure model given in Fig. 5 with positional parameters Ba: 0,0,0 and 0,0,0.190; Pb: 0.5,0.5,0.09; O: 0.5,0.5,0, 0.5,0,0.09, and 0.5,0.5,0.19 (Ref. 10) with cell dimensions of $a = 4.29$, $c = 21.7$ Å and spacegroup $I4/mmm$. The calculated image is given as an inset in Fig. 4. Figure 5 summarizes the crystal structures and chemistry of all the presently known members of the $(Ba,K)_{n+1}(Pb,Bi)_nO_{3n+1}$ homologous series.

PHYSICAL CHARACTERIZATION

In order to make an initial comparison of the properties of the members of the $Ba_{n+1}Pb_nO_{3n+1}$ series, we

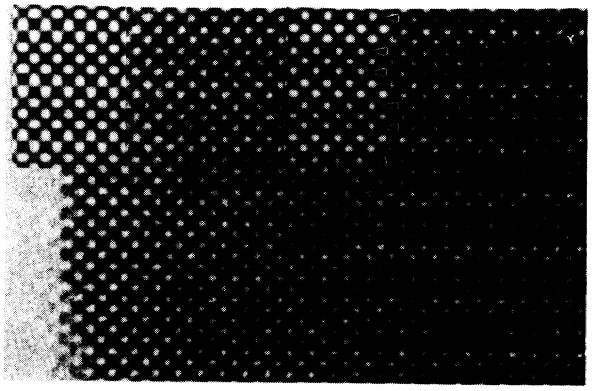

FIG. 4. [110] micrograph of $Ba_3Pb_2O_7$. Arrows point to the Pb atom columns. Calculated images at a defocus of -40 nm and thicknesses of 2 nm (left) and 6 nm (right) are given as insets.

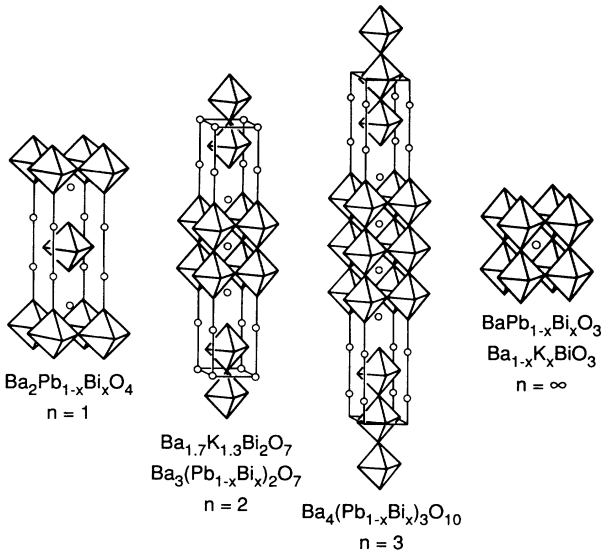

FIG. 5. All the presently known members of the $(Ba,K)_{n+1}(Pb,Bi)_nO_{3n+1}$ homologous series.

present in Fig. 6 the temperature-dependent resistivities of polycrystalline materials for all the presently known members $n = 1$, 2, 3, and ∞. The firing temperatures in oxygen for sintering the samples of Ba_2PbO_4 $Ba_4Pb_3O_{10}$, and $BaPbO_3$ were 1025, 950, and 850 °C, respectively. All were then fired in oxygen at 450 °C overnight and found to be single phase by powder x-ray diffraction. The results show a systematic trend to higher resistivity with increasing two-dimensionality. The band-structure calculations made for this series[11] showed the very small overlap between the nonbonding O $2p$ and Pb $6s$–O $2p$ σ^* energy bands to decrease on going from $BaPbO_3$ to $Ba_4Pb_3O_{10}$, and that a band gap was expected to open for $Ba_3Pb_2O_7$, becoming approximately 1.7 eV for Ba_2PbO_4. Our observations are essentially consistent with the band calcula-

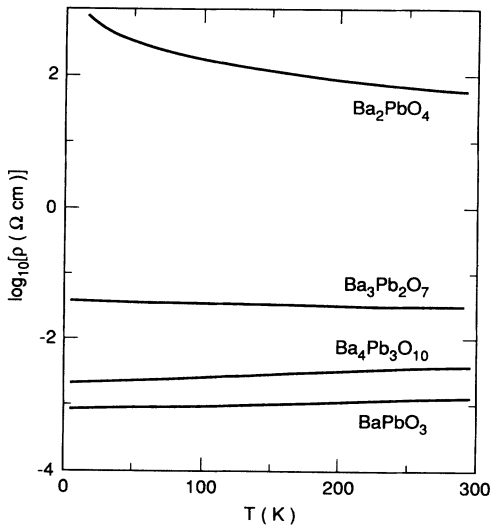

FIG. 6. Temperature dependence of the resistivity for polycrystalline $BaPbO_3$, $Ba_4Pb_3O_{10}$, $Ba_3Pb_2O_7$, and Ba_2PbO_4.

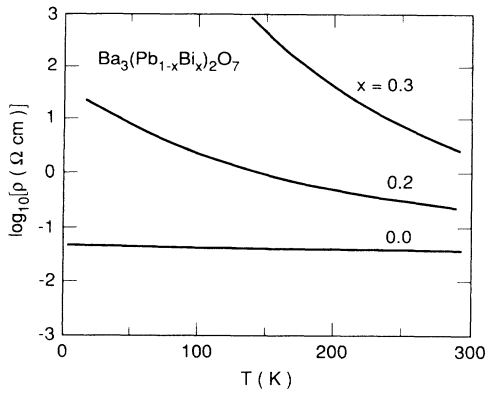

FIG. 7. Temperature dependence of the resistivity for polycrystalline $Ba_3(Pb_{1-x}Bi_x)_2O_7$ for $x=0.0$, 0.2, and 0.3.

tions. Because of the expected semimetallic or semiconducting properties, however, very small amounts of electronically active defects, e.g., oxygen vacancies, would be expected to have a significant effect on the observed resistivities. The poorly metallic nature of the compound $Ba_3Pb_2O_7$ therefore may be explained in terms of electronically active defects.

The resistivities for polycrystalline pellets of the single-phase compositions $Ba_3(Pb_{1-x}Bi_x)_2O_7$ $x=0$, $0.2 \leq x \leq 0.5$, were measured in a conventional four-probe configuration between 300 and 4.2 K. The results are summarized in Fig. 7. In this class of compounds, Bi substitution would provide electrons to a Bi 6*s*, Pb 6*s*–O 2*p* σ^* band within a naive rigid-band picture. However, in $n=\infty$ $BaPb_{1-x}Bi_xO_3$, an increasing instability against charge-density-wave (CDW) formation and/or increasing disorder upon Bi substitution influences the conductivity strongly: the material becomes more resistive and finally experiences a metal-to-semiconductor transition. The same trend is clearly seen in the present $Ba_3(Pb_{1-x}Bi_x)_2O_7$ compound (Fig. 7). The detrimental effect of Bi substitution on the conductivity is much more pronounced than for $BaPb_{1-x}Bi_xO_3$. The $x=0.2$ and 0.3 samples, which have approximately the same number of electrons per (Pb·Bi) as does superconducting $BaPb_{0.75}Bi_{0.25}O_3$, are already insulating, showing a variable range-hopping-type temperature-dependent resistivity.

As is evident from Fig. 7, no trace of superconductivity was observed down to 4.2 K in the resistivity measurements. The polycrystalline samples were further tested for superconductivity in a SQUID magnetometer by cooling in a field of 10 Oe down to a temperature of 1.8 K. We did not, however, observe any Meissner signal within our sensitivity limits.

CONCLUSIONS

With this report of the synthesis of $Ba_3(Pb_{1-x}Bi_x)_2O_7$, the $n=1$, 2, 3, and ∞ members of the $Ba_{n+1}(Pb_{1-x}Bi_x)_nO_{3n+1}$ series are now known. All can be doped, at least by a naive chemical picture, to an electron concentration, ~ 0.25 electron per (Pb·Bi), which is optimal for superconductivity for the $n=\infty$ $BaPb_{1-x}Bi_xO_3$ simple perovskite. The layered materials do not become superconducting, even the $n=3$ material which is not, on casual inspection, much different from the three-dimensional perovskite.[8]

The reason that the reduced dimensionality is so detrimental in this class of materials has not yet been determined. The reduced dimensionality changes the parent compound from a semimetal to a semiconductor and makes the effects of Bi substitution (chemically electron doping) less electronically active. This could be due to the increased tendency toward CDW formation in lower dimensions, or increased effects of disorder introduced by Bi/Pb mixing in lower dimensions. Band-structure calculations have lead to the proposal[11] that in the lowest unoccupied states (at $x=0$) are of apical oxygen character rather than in-plane oxygen character as is found for $Ba(Pb_{1-x}Bi_x)O_3$, resulting in a change in character of the conduction band. Further quantitative physical characterization of this family of materials will be necessary to resolve these issues and establish why their behavior is so different from that of copper oxides.

[1]A. W. Sleight, J. L. Gillson, and P. E. Bierstedt, Solid State Commun. **17**, 27 (1975).
[2]R. J. Cava, B. Batlogg, J. J. Krajewski, R. Farrow, L. W. Rupp, Jr., A. E. White, K. Short, W. F. Peck, Jr., and T. Kometani, Nature (London) **332**, 814 (1988).
[3]R. J. Cava, B. Batlogg, G. P. Espinosa, A. P. Ramirez, J. J. Krajewski, W. F. Peck, Jr., L. W. Rupp, Jr., and A. S. Cooper, Nature (London) **339**, 291 (1989).
[4]B. Batlogg *et al.*, Phys. Rev. Lett. **61**, 1670 (1988).
[5]D. G. Hinks, D. R. Richards, B. Dabrowski, D. T. Marx, and A. W. Mitchell, Nature (London) **335**, 419 (1988).
[6]C. M. Varma, Phys. Rev. Lett. **61**, 2713 (1988).
[7]V. G. Wagner and H. Binder, Z. Anorg. Allg. Chem. **298**, 12 (1959).
[8]W. T. Fu, H. W. Zandbergen, Q. Xu, J. M. van Ruitenbeek, L. J. de Jongh, and G. van Tendeloo, Solid State Commun. **70**, 1117 (1989).
[9]M. Licheron and F. Gervais, Mater. Sci. Eng. B **6**, 61 (1990).
[10]R. J. Cava, T. Siegrist, W. F. Peck, Jr., J. J. Krajewski, B. Batlogg, and J. Rosamilia, Phys. Rev. B **44**, 9746 (1991).
[11]L. F. Mattheiss, Phys. Rev. B **42**, 359 (1990).

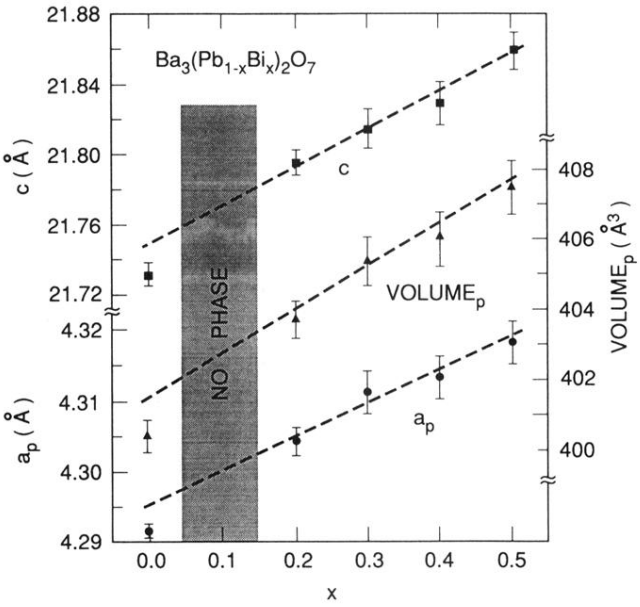

FIG. 1. Variation of the crystallographic cell parameters (*I*4/*mmm* perovskite-like subcell) with Bi content in $Ba_3(Pb_{1-x}Bi_x)_2O_7$.

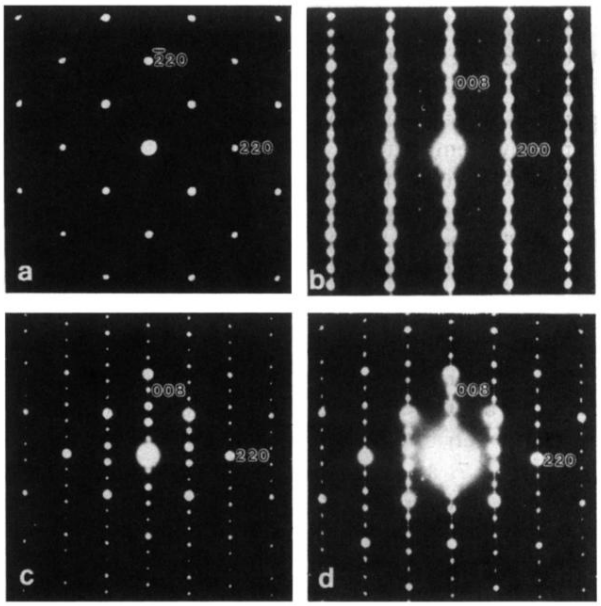

FIG. 2. Electron-diffraction patterns along (a) [001], (b) [100], (c) [110], and (d) [110]. Note the superstructure along the c^* axis in (d), which probably corresponds to a stacking of five units of $Ba_3Pb_2O_7$ and one unit of $Ba_4Pb_3O_{10}$. Streaking corresponding to irregular stacking defects can be seen in (b) and (c).

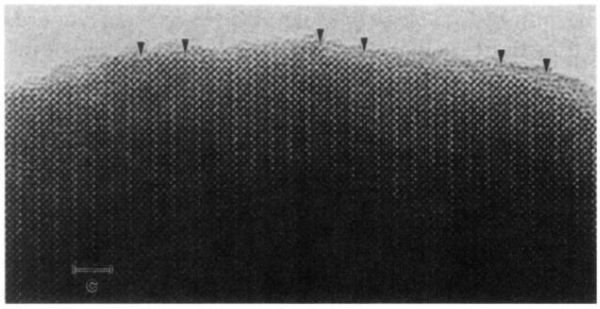

FIG. 3. [110] micrographs showing the presence of a stacking defects corresponding to a composition $Ba_4Pb_3O_{10}$ (arrows) in a matrix of $Ba_3Pb_2O_7$. Note that the defects in the matrix have a regular sequence $[6x(Ba_3Pb_2O_7)1x(Ba_4Pb_3O_{10})1x(Ba_3Pb_2O_7)1x(Ba_4Pb_3O_{10})]_n$.

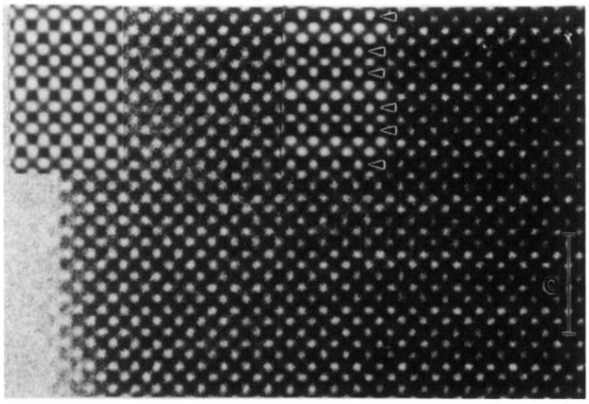

FIG. 4. [110] micrograph of $Ba_3Pb_2O_7$. Arrows point to the Pb atom columns. Calculated images at a defocus of -40 nm and thicknesses of 2 nm (left) and 6 nm (right) are given as insets.